

# Implementation of an iterative quantum order finding algorithm

Enrique Martín López,<sup>\*</sup> Anthony Laing,<sup>\*</sup> Thomas Lawson,<sup>\*</sup> Roberto Alvarez, Xiao-Qi Zhou, and Jeremy L. O'Brien<sup>†</sup>  
*Centre for Quantum Photonics, H. H. Wills Physics Laboratory & Department of Electrical and Electronic Engineering,  
 University of Bristol, Merchant Venturers Building, Woodland Road, Bristol, BS8 1UB, UK*

Quantum algorithms are computational routines that exploit quantum mechanics to solve problems exponentially faster than the best classical algorithms. The quantum order finding algorithm is a key example—it is the subroutine that delivers the exponential speed-up in Shor's factoring algorithm. To date, the demand on quantum resources—qubits and logic gates—even for small instances, has meant that there have been only four experimental realisations. We demonstrate a scalable, iterative order finding algorithm that uses one third the number of qubits in a scalable way. Encoding in higher-dimensional states, we implement a two-photon compiled algorithm for which the algorithmic output exhibits structure that is sensitive to noise, in contrast to previous demonstrations. These results point to larger-scale implementations of Shor's algorithm by harnessing substantial but scalable resource reductions applicable to all physical architectures.

Developing more powerful computers is an ongoing technological challenge, however some tasks consume exponential computational resources, putting large instances forever beyond the capability of conventional computers. In contrast, quantum computers [1–3] promise to be able to address some of these intractable tasks with only polynomial resources. The exponentially greater power offered by Shor's quantum factoring algorithm [4] over the best known classical methods, for example, has fuelled a major international effort to realise such a device [5]. Despite this great promise, to date, there have been only four demonstrations [6–9], due to the large number of resources required even for such small-scale demonstrations.

We implement a scalable iterative order finding algorithm [10] that reduces the number of qubits in the control register to one, in a scalable way. Focussing on the case of factoring 21, we take advantage of the higher dimensional encoding that is straightforwardly available with photons and use a single three-level photonic qutrit in the work register. Even with these substantial reductions in the number of quantum systems, our two photon scheme still requires two consecutive photonic controlled-not (CNOT) gates—something that has not previously been demonstrated—acting on different subspaces of the qutrit respectively. We observe a probability distribution that is non-uniform, in contrast to factoring 15 [6–9]—an example of an algorithm whose (correct) output distribution is uniform, making it insensitive to decoherence.

In Shor's factoring algorithm (see, for example, [3]), to determine the prime factors of an odd integer  $N$ , one chooses a co-prime of  $N$ ,  $x$ . The integer  $r$ , known as the order, which relates  $x$  to  $N$  according to  $x^r \bmod N = 1$ , can be used to obtain the factors, given by the greatest common divisor  $\gcd(x^{\frac{r}{2}} \pm 1, N)$ . The algorithm thus consists of an order finding algorithm, preceded and succeeded by various classical tasks, which perform checks ensuring  $x$  and  $N$  are appropriate and are responsible for extracting the factors from  $r$ . While the classical tasks are known to be efficient on a classical computer, order

finding is understood to be intractable classically. However, it is known that this part of the algorithm can be performed efficiently on a quantum computer.

The quantum order finding circuit involves two registers: a work register and a control register. In the standard protocol, the work register performs modular arithmetic with  $m = \lceil \log_2 N \rceil$  qubits, enough to encode the number  $N$ , and an  $n$  qubit control register that provides the algorithmic output, with  $n$  bits of precision [20]. For large  $n$ , and a perfectly functioning circuit, the output probability distribution of the control register is a series of well defined peaks at values of  $k/r$  (Fig. 1(b)). Therefore, after the protocol is complete, with high probability, measurement of the control register gives the first  $n$  bits of  $k/r$ , where  $0 \leq k \leq r - 1$  occurs randomly, according to the laws of quantum mechanics.

Despite being the primary application motivating efforts to realise a quantum computer, the large number of qubits and logic gates required to implement Shor's algorithm has meant that demonstrations have so far been confined to factoring 15 [6–9]. In the iterative version of the order finding algorithm [10] the control register contains only a single qubit which is recycled  $n$  times, using a sequence of measurement and feed-forward operations, with each step providing an additional bit of precision (Fig. 1(a)). (The iterative version of the order finding algorithm is closely related to the semi-classical picture of the quantum Fourier transform [11].) This simple and scalable modification substantially reduces the total number of qubits required from  $\lceil 3 \log_2 N \rceil$  to  $\lceil \log_2 N \rceil + 1$ . The only penalty is a polynomial increase in computation time, while the exponential speedup is retained—*i.e.* it is scalable. (Note that this multiplicative saving in qubits results in an exponential reduction in Hilbert space.)

As the number of control qubits, or iterations,  $n$  is reduced, in general, the precision is reduced and the  $k$  peaks in the probability distribution become smeared, as shown in Fig. 1(b). However, in the special case where the order is a power of two and  $r = 2^p$ , the peaks corre-

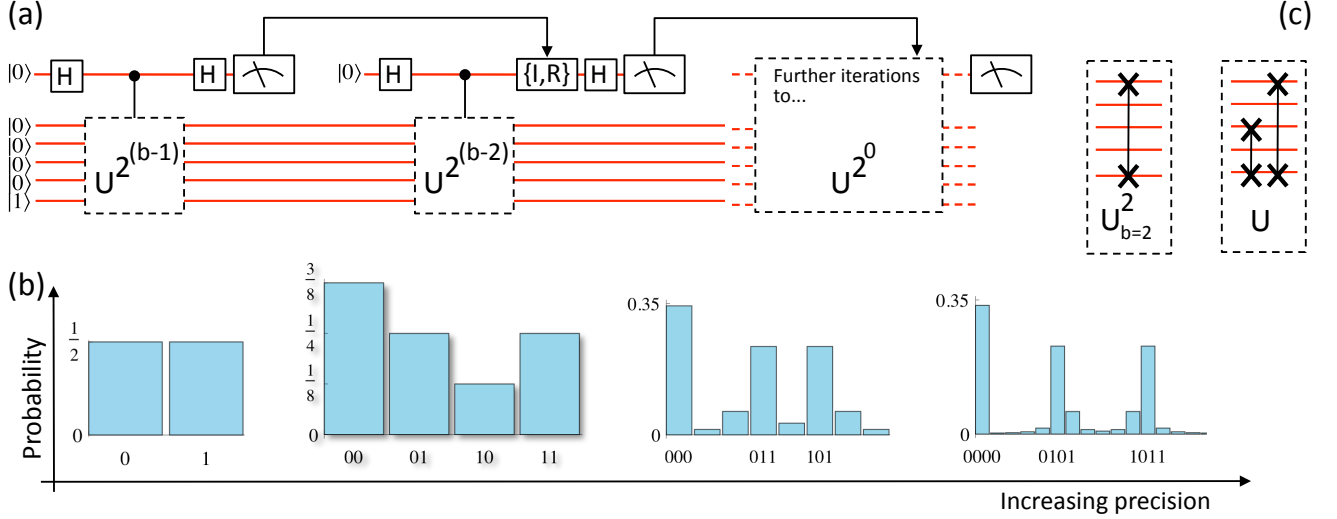


FIG. 1: The iterative order finding algorithm for factoring 21. (a) Measurement of the control qubit after implementation of each controlled unitary gives the next most significant bit in the output and the outcome is fed forward to the iterated (semi-classical) Fourier transform, which implements either the identity  $I$  or the appropriate phase gate  $R$ , prior to the Hadamard  $H$ . (b) As the number of iterations increases the precision increases. (c) For two bits of precision the controlled unitary operations can be implemented with this arrangement of controlled-swap gates.

spond exactly to the logical states of  $p$  qubits [21] such that the output is equivalent to that of an incoherent mixture of  $p$  qubits (any additional control qubits remain unentangled throughout the algorithm and simply encode the trailing zeros in the uniform distribution). Factoring  $N = 15$  [6–9] gives either order 2 or order 4 for each of its co-primes; independent verification of entanglement is therefore required [7, 8]. For this reason we focus on  $N = 21$  with the co-prime  $x = 4$  to give  $r = 3$  [22]. To two bits of precision the expected outcomes 00, 01, 10 and 11 occur with probabilities  $\frac{3}{8}$ ,  $\frac{1}{4}$ ,  $\frac{1}{8}$  and  $\frac{1}{4}$ , respectively (Fig 1(b)). The underlying periodic structure is apparent in this distribution, which is susceptible to decoherence.

To realise this case, we implement a scalable iterative quantum algorithm with a compiled version of the quantum order finding routine, where the explicit form of the unitary operators is assumed to be known in order to simplify their construction [6–9, 12]. In the standard qubit encoding, the work register requires enough qubits to represent  $N$  in binary. However, as only three terms in the binary series are ever accessed during the order finding algorithm for  $N = 21$  we take advantage of the higher levels available in photon path and polarisation encoding and use a single qutrit in the work register, as shown in Fig. 2(a), rather than two qubits [23]. The first two controlled-SWAP operations are implemented as controlled-NOT (CNOT) gates, acting on different qubit subspaces of the qutrit work register, and the third with an uncontrolled swap gate, equivalent to a relabelling of two modes of the qutrit, to realise the effective opera-

tion of the third controlled-SWAP. In our experimental implementation we use the iterative approach with post-selection in place of measurement and feed-forward; measurement and feed-forward operations have been achieved in the context of cluster state quantum computing with photons [13].

The quantum order finding circuit of Fig. 2(a) was implemented using the optical circuit shown schematically in Fig. 2(b). Implementing two consecutive CNOT gates on two photons was achieved by using an entanglement driven CNOT gate (eCNOT) [14], followed by a post-selected CNOT gate (pCNOT) [15–18] (pCNOT gates cannot be used in series without the addition of ancilla photons). The circuit was implemented with Jamin-Lebedeff polarisation interferometers in a calcite beam displacer architecture, chosen to provide interferometric stability; further details are given in the *Appendix*. Photons were generated with a polarisation entangled spontaneous parametric down conversion source [19], details of which are given in the *Appendix*.

The correct algorithmic output from the quantum order finding circuit for factoring  $N = 21$  is confirmed by the data shown in Fig. 3(a). The two-qubit control register output probabilities for 00, 01, 10 and 11 were measured and found to have a fidelity of  $99 \pm 4\%$  [24] with the ideal probabilities  $\frac{3}{8}$ ,  $\frac{1}{4}$ ,  $\frac{1}{8}$  and  $\frac{1}{4}$ , respectively. The distribution on the first qubit, which determines the second bit in the total probability distribution, was measured by comparing total control register counts, heralded by the  $W(2)$  detector, for each setting of the first qubit projector (stage (2) of the circuit in Fig. 2(b)) and found to be

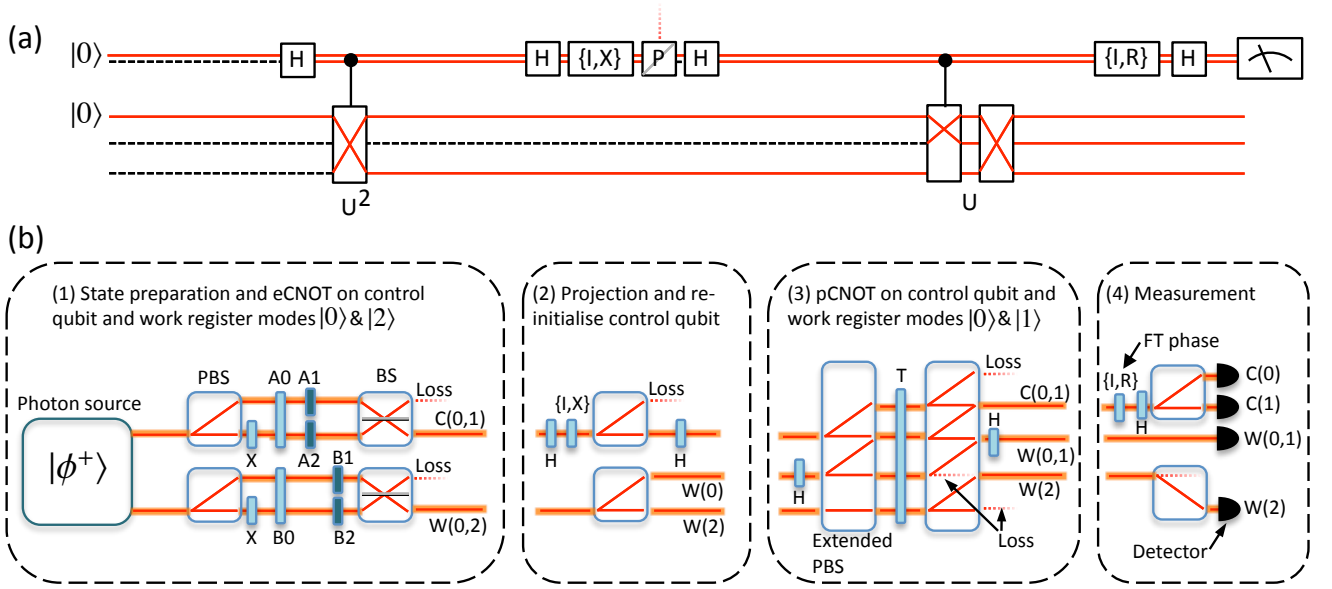


FIG. 2: Compiled iterative order finding algorithm. (a) Idealised compiled circuit diagram. The first controlled unitary is implemented as a CNOT acting on work modes 0 and 2; the final controlled unitary uses a CNOT on work modes 0 and 1 followed by an uncontrolled swap on work modes 0 and 2.  $P$  indicates a projection onto the computational 0, preceded by either a bit flip gate  $X$ , or the identity  $I$ ;  $H$  denotes the Hadamard gate. The iterative Fourier transform includes the rotation  $R = |H\rangle\langle H| - i|V\rangle\langle V|$  when the first projection is made on to the computational 1 state. (b) Schematic of the experimental circuit (see *Appendix* for details).

uniform with fidelity  $99 \pm 5\%$  (Fig. 3(b)).

Since the non-uniformity of the distribution of Fig. 3(a) arises from the second iteration of the algorithm when the first iteration gives output zero, we now focus on this case. Analysis of the circuit and algorithm reveal a critical dependence on decoherence, particularly in the pCNOT and the Fourier transform phase: phase instability drives the output toward a uniform probability distribution. We confirmed this analysis experimentally, as described below.

With stage 2 of the circuit set so that the first qubit is projected onto the computational zero state Figs. 3(c) and 3(d) show 16 probability distributions for the correct phase setting (*i.e.* 0) to implement the semiclassical Fourier transform and 15 incorrect settings of this phase. When heralded by the detector that does not distinguish between the 0 and 1 states of the work qutrit, the control qubit should be in a maximal mixture and therefore insensitive to this phase—*i.e.* give a flat line response. In contrast, since mode 2 of the qutrit is not involved in the final CNOT gate, the control qubit is not entangled with it. Therefore, when heralded by the work qutrit being in the 2 state, the control photon should be in a pure state and should exhibit maximum sensitivity to the phase in the Fourier transform—*i.e.* a unit visibility fringe. Taking into account the relative probability amplitudes in the ideal output state, the ideal plot of probability distributions would show two sinusoidal curves of full visibility (from detectors  $C(0)&W(2)$  and  $C(1)&W(2)$ ) each bi-

sected by a flat line (from detectors  $C(0)&W(0,1)$  and  $C(1)&W(0,1)$ ). For the 8 probability distributions between two settings of the Fourier transform phase, 0 and  $\pi$  (indicated by black vertical lines) we find an average fidelity between this situation and our data of  $91.6 \pm 0.6\%$ .

The data in Figs. 3(c) and 3(d) can be used to show the sensitivity of the circuit to decoherence: Integrating the probability distribution over the range 0 to  $\pi$  of the Fourier transform phase simulates the effect of phase instability. The red distribution plotted in Fig. 3(e) shows the near uniform distribution that results from this procedure, confirming susceptibility of this circuit to decoherence.

Scalable reduction of the number of qubits in the order finding algorithm via the iterative approach opens the way to larger scale demonstrations of Shor's factoring algorithm in all physical implementations. In some of these implementations recycling of the control qubit will be more straightforward. In cases where two qubit gates can be realised deterministically, scaling to factoring of larger numbers becomes more tractable. Encoding in higher-dimensional systems in a scalable way is promising for the many implementations where higher levels or other degrees of freedom are available.

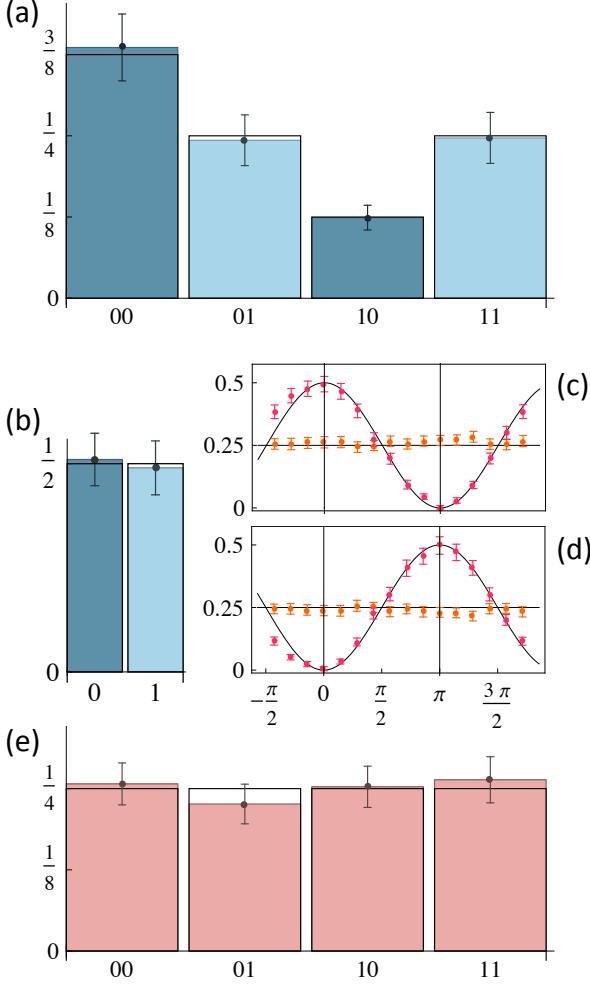


FIG. 3: Demonstration of order finding. Ideal probability distributions are plotted in solid black lines. (a) The two-bit output probability distribution for the order finding algorithm. (b) Output from the first iteration of the order finding algorithm. (c) & (d) Probability distributions for 16 phases of the Fourier transform, as described in the text, for control qubit detectors 0 and 1 respectively. (e) The distribution obtained from experimental simulation of decoherence in the Fourier transform. Data were corrected for the measured difference in total coupling efficiency between the work register detectors.

## Appendix

**Photon source:** The photon source was a Type 1 spontaneous parametric down conversion source, in which a 404 nm CW laser was focused to a 40  $\mu\text{m}$  waist in a pair of crossed  $\text{BiB}_3\text{O}_6$  (Bismuth Triborate) non linear crystals to produce entangled pairs of photons [19] spectrally degenerate at 808nm. The entangled photon-pairs were spectrally filtered with high transmission interference filters of FWHM 3nm, then collected into polarisation maintaining optical fibres (PMFs). PMFs would

normally decohere the polarisation of photons that are not aligned with the slow or fast axis of the fibre, as is the case for photons that are entangled. Our fibres were cut at the midpoint and spliced together with a 90 degree twist such that the slow axis in the first length was aligned with the fast axis in the 2nd length. While this modified fibre imparts an unknown phase shift between the two polarisations, their coherence is preserved. The unknown unitary is pre-compensated with waveplates in the source. State tomography of the photon source, which drives the eCNOT gate, revealed a highly entangled state with fidelity  $96.9 \pm 0.2\%$  to the corresponding Bell state [25].

**Optical Circuit:** The optical circuit of Fig. 2(b) was implemented using an architecture of calcite beam displacers (BD), which separate the ordinary and extraordinary polarisations and can be used to form very stable Jamin-Lebedeff interferometers—polarisation interferometers with parallel light-paths that provide interferometric stability. The PBSs and Extended PBSs in Fig 2 were directly implemented with a single BD. The eCNOT gate [14] requires two non polarising 50% reflectivity beam splitters (BS in Fig 2) the unitary operation of which was constructed with four BDs and waveplates. The action of polarisers A1 and A2 was implemented using beam stops after the first BD in the BSs. The operation of the circuit is as follows:

*Stage 1:* Input states are prepared with the A0 and B0 waveplates, which are chosen to be the Hadamard (H) and Identity (I) respectively. The controlled-unitary gate is driven by a polarisation-entangled photon source, which is then converted to spatial entanglement via the polarising beam splitters (PBS) and polarisation flip (X) waveplates. In its general form, this gate can perform any controlled unitary operation. Setting the controlled-unitary to perform the CNOT requires A1 and A2 to be polarisers which pass vertical and horizontal polarisations respectively. B1 and B2 are required to be I and X, respectively. When the control exit port and work exit port of the BSs each contain a photon, the CNOT gate logic has been performed. The polarisation modes within the control spatial mode correspond to the qubit computational states indicated by  $C(0,1)$ ; at this point the polarisation modes within the work spatial mode correspond to the  $|0\rangle$  and  $|2\rangle$  qutrit states, indicated by  $W(0,2)$ .

*Stage 2:* The control qubit is projected onto one of the computational states, dependent upon whether  $I$  or  $X$  is implemented before the upper PBS. The lower PBS introduces the third mode for the work register so that the  $|0\rangle$  and  $|1\rangle$  states are polarisation encoded in the upper spatial mode of the work register (though at this stage the  $|1\rangle$  state has zero probability amplitude, i.e. vacuum) while the lower spatial mode contains only one polarisation and corresponds to the  $|2\rangle$  state.

*Stage 3:* The pCNOT gate relies on photonic quan-

tum interference tuned by the half waveplate  $T$  which is set to  $62.5^\circ$ . Successful operation is heralded when one photon is present in the control modes and one photon is present in the work modes. Here, further balancing loss is introduced into the  $W(2)$  mode. The output from  $W(2)$  and the usual pCNOT work loss mode share the same spatial mode but different polarisations. The entangling capability of the pCNOT gate was tested with a Bell inequality violation (while in situ) recording a CHSH value of  $2.67 \pm 0.01$  (violating the classical limit of 2 by 55 standard deviations).

*Stage 4:* The control qubit is assigned a phase according to the projector in the first iteration, allowing implementation of the semi-classical Fourier transform. The control qubit states are individually projected and provide the order finding results. At the final stage, the work qutrit plays no role in providing order finding information (other than to herald the control qubit) so individual computational states may be traced out in detection. The polarisations of the upper work spatial mode are not distinguished, but the remaining work mode is; these two cases provide a useful method to confirm correct circuit operation.

We thank Stephen Bartlett, Richard Jozsa, Gary McConnell, Tim Ralph, Terry Rudolph and Pete Shadbolt for helpful discussions. This work was supported by EPSRC, ERC, PHORBITECH and NSQI. J.L.O'B. acknowledges a Royal Society Wolfson Merit Award.

---

\* These authors contributed equally to this work

† Electronic address: Jeremy.O'Brien@bristol.ac.uk

- [1] R. P. Feynman, Int. J. Thy. Phys. **21**, 467 (1982).
- [2] D. Deutsch, Proc. R. Soc. Lond. A **400**, 97 (1985).
- [3] M. A. Nielsen and I. L. Chuang, *Quantum Computation and Quantum Information* (Cambridge University Press, 2000).
- [4] P. W. Shor, Proc. 35th Annu. Symp. Foundations of Computer Science and IEEE Computer Society and Los Alamitos and CA pp. 124–134 (1994), ed. S. Goldwasser.
- [5] T. D. Ladd, F. Jelezko, R. Laflamme, Y. Nakamura, C. Monroe, and J. L. O'Brien, Nature **464**, 45 (2010).
- [6] L. M. K. Vandersypen, M. Steffen, G. Breyta, C. S. Yannoni, M. H. Sherwood, and I. L. Chuang, Nature **414**, 883 (2001).
- [7] C.-Y. Lu, D. E. Browne, T. Yang, and J.-W. Pan, Phys. Rev. Lett. **99**, 250504 (2007).
- [8] B. P. Lanyon, T. J. Weinhold, N. K. Langford, M. Barbieri, D. F. V. James, A. Gilchrist, and A. G. White, Phys. Rev. Lett. **99**, 250505 (2007).
- [9] A. Politi, J. C. F. Matthews, and J. L. O'Brien, Science **325**, 1221 (2009).
- [10] S. Parker and M. B. Plenio, Phys. Rev. Lett. **85**, 3049 (2000).
- [11] R. B. Griffiths and C.-S. Niu, Phys. Rev. Lett. **76**, 3228 (1996).
- [12] D. Beckman, A. N. Chari, S. Devabhaktuni, and J. Preskill, Phys. Rev. A **54**, 1034 (1996).
- [13] R. Prevedel, P. Walther, F. Tiefenbacher, P. Bohi, R. Kaltenbaek, T. Jennewein, and A. Zeilinger, Nature **445**, 65 (2007).
- [14] X.-Q. Zhou, T. C. Ralph, P. Kalasuwan, M. Zhang, A. Peruzzo, B. P. Lanyon, and J. L. O'Brien, Nat. Commun. **2**, 413 (2011).
- [15] T. C. Ralph, N. K. Langford, T. B. Bell, and A. G. White, Phys. Rev. A **65**, 062324 (2001).
- [16] H. F. Hofmann and S. Takeuchi, Phys. Rev. A **66**, 024308 (2001).
- [17] J. L. O'Brien, G. J. Pryde, A. G. White, T. C. Ralph, and D. Branning, Nature **426**, 264 (2003).
- [18] J. L. O'Brien, G. J. Pryde, A. Gilchrist, D. F. V. James, N. K. Langford, T. C. Ralph, and A. G. White, Phys. Rev. Lett. **93**, 080502 (2004).
- [19] P. G. Kwiat, E. Waks, A. G. White, I. Appelbaum, and P. H. Eberhard, Phys. Rev. A **60**, 773 (1999).
- [20] In the standard implementation setting  $\log(N^2) \lesssim n \lesssim \log(2N^2)$  guarantees correct output with high probability.
- [21] In fact the same is generally true of a control register based on  $d$  dimensional systems (qudits) and orders that are a power of  $d$ ,  $r = d^p$ .
- [22] Shor's algorithm is designed to work for even orders only, as the classical subroutine must calculate  $\gcd(x^{\frac{N}{2}} \pm 1, N)$ . However, for certain choices of square coprime  $x$  and odd order, the algorithm works. For example, in the case of  $x = 2^{2j}$  with  $j$  an integer, a numerical simulation of Shor's algorithm for the first (odd) 4851 composite  $N$  (product of two primes) finds approximately 58% of this class of coprimes produces an odd order; of these approximately 36% successfully lead to non trivial factors of  $N$  in the classical gcd subroutine. Order finding for  $N = 21$  with  $x = 4$ , resulting in  $r = 3$  is one such successful example.
- [23] Note that, while encoding in higher dimensions will reduce the number of required photons, encoding the entire work register in a single  $s$ -level system typically requires resources exponential in  $n$ .
- [24] All fidelities are calculated as  $1 - \text{trace distance}$ . The *trace distance* between two probability distributions  $\{p_x\}$  and  $\{q_x\}$  (sometimes known as the  $L_1$  distance or *Kolmogorov distance*) is defined by the equation  $D(p_x, q_x) \equiv \frac{1}{2} \sum_x |p_x - q_x|$  [3].
- [25] Fidelity between two quantum states  $\rho$  and  $\sigma$  is defined to be  $F(\rho, \sigma) \equiv \text{Tr} \sqrt{\rho^{1/2} \sigma \rho^{1/2}}$  [3].